Optik - International Journal for Light and Electron Optics 287 (2023) 171162

Contents lists available at ScienceDirect

Optik

journal homepage: www.elsevier.com/locate/ijleo

Symmetrical dual D-shape fiber for waveguide coupled surface plasmon resonance sensing

Jianxin Wang [a], Wei Liu [a], Lin Yang [a], Jingwei Lv [a], Qianqian Yin [a], Qiang Liu [a], Yan Lv [a], Paul K. Chu [b], Chao Liu [a,*]

[a] School of Physics and Electronic Engineering, Northeast Petroleum University, Daqing 163318, PR China
[b] Department of Physics, Department of Materials Science and Engineering, and Department of Biomedical Engineering, City University of Hong Kong, Tat Chee Avenue, Kowloon, Hong Kong, PR China

ARTICLE INFO

Keywords:
Waveguide coupled surface plasmon resonance
Single-mode fiber
Dual D-shape fiber
Full-width at half-minimum

ABSTRACT

A waveguide-coupled surface plasmon resonance (WCSPR) sensor consisting of two D-shape single-mode fibers is designed and analyzed by the finite element method (FEM). The optical field of the surface plasmon polaritons (SPPs) mode is confined in the dielectric cavity between the dual metallic thin films. Therefore, the effective refractive index of the SPP mode depends largely on the refractive index of the analyte and an anomalous dispersion relationship is observed between the SPP mode and x-polarized core-guide mode of the dual D-shape fiber. The excitation mechanism of surface plasmon resonance (SPR) in the coupling region is attributed to phase matching of the two modes. Further analysis shows that the narrow bandwidth peak in the loss spectrum of the core mode is determined by the sensor dimensions contributed jointly by the thicknesses of the silver film, dielectric layer, and titanium dioxide film. Compared to the single-fiber structure, the optimized dual D-shape WCSPR sensor achieves a maximum wavelength sensitivity of 52,200 nm/RIU with a full-width at half-minimum (FWHM) of 9.47 nm and a figure of merit (FOM) of 346.6 RIU^{-1} in the analyte refractive index range of 1.32–1.42.

1. Introduction

Surface plasmon resonance (SPR) is a physical phenomenon that involves the excitation of surface plasmon polaritons (SPPs), which are collective oscillations of free charges at the interface between a noble metal and dielectric materials [1]. Owing to the unique properties such as label-free monitoring, high sensitivity, and real-time detection, SPR has garnered widespread interest and is used in optical devices including filters [2–4], optical absorbers [5,6], fiber optic sensors [7], and optical instruments [8,9]. Furthermore, the dependence of SPPs on the refractive index of the adjacent dielectrics renders SPR sensors ideal for a myriad of applications encompassing biochemistry [10], industrial detection [11], and water and food safety inspection [12]. However, high sensitivity and high factor of merit (FOM) are often not obtained simultaneously due to the limitations of conventional SPR sensing techniques.

In order to address this limitation, researchers have investigated alternative SPR modes, such as local SPR (LSPR), long-range SPR (LRSPR) [13–15], coupled plasmon waveguide resonance (CPWR) [16], and waveguide coupled SPR (WCSPR) [17–19]. Recently, LSPR sensors developed based on optical fibers show exaggerated sensitivity and FOM values, demonstrating great potential for applications in the field of refractive index sensing [20–23]. Among them, Pathak et al. embedded gold nanowires into a drilled

* Corresponding author.
E-mail address: msm-liu@126.com (C. Liu).

https://doi.org/10.1016/j.ijleo.2023.171162
Received 25 May 2023; Received in revised form 5 July 2023; Accepted 10 July 2023
Available online 13 July 2023

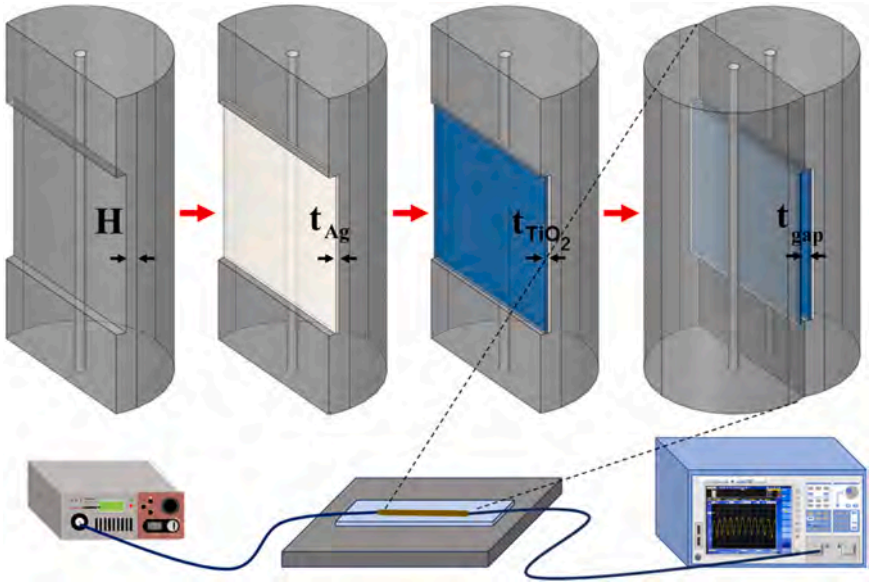

Fig. 1. Proposed sensor fabrication process and general setup for measurement experiments.

single-mode fiber to achieve LSPR excitation and obtain ultra-high sensing sensitivity of over 90,000 nm/RIU [22]. Ma et al. designed a multilayer plasma structure based on a platinum (Pt) grating for LSPR excitation, and the numerical structure showed a high FOM value of 432 RIU-1 and a high refractive index sensitivity of 11,252 nm/RIU in the refractive index range of 1.33–1.41 [20]. However, these structures rely on nanowires or gratings to achieve LSPR excitation, which makes fabrication difficult and costly to control.

Conventional LRSPR fiber sensors are constructed by adding a dielectric buffer layer (DBL) to create a refractive index environment inside and outside the metal layer that is identical [24]. This enables the propagation length of SPP to exceed the conventional propagation length, resulting in a significant improvement of signal-to-noise ratio and resolution at the interrogated wavelength. However, due to the highly dependent performance of the sensors on the existence of a symmetric environment, it is not easily applicable to different detection environments related to various biological molecules or buffer solutions. Of interest is that the LRSPR sensor designed based on photonic crystal fiber (PCF) achieves a refractive index sensitivity of 14,700 nm/RIU and a FOM of 475 RIU^{-1} without adding a DBL layer [25]. However, the overly complex fiber optic structure hinders the implementation of PCF sensors, and the complexity of the fabrication process and the presence of problems such as high errors lead to expensive production and low success rates of MOF sensors [26].

CPWR sensors, on the other hand, add a high refractive index dielectric layer as a waveguide layer to the surface of a conventional SPR sensor [10]. The presence of waveguide resonance modes typically results in loss curves with lower FWHM and higher signal-to-noise ratio. However, due to the increased distance between the metal film and the analyte, the sensing sensitivity is lower than that of conventional SPR sensor. A common feature of WCSPR sensor is the addition of a waveguide layer between two metal layers [10]. When SPP is excited at the metal-waveguide interface, they couple into symmetric and asymmetric modes in the waveguide layer and then couple back to the SPP mode excited at the metal-dielectric interface. Therefore, in WCSPR devices, the symmetric mode produces a sharper resonance peak, improving measurement accuracy while maintaining sensitivity similar to that of traditional SPR sensors.

Here, we investigate a WCSPR sensor for refractive index detection, which consists of two common D-shape single-mode fibers with Ag and TiO_2 plasmonic materials coated on the surface of the exposed core. The sensor fabrication process is based on proven fiber optic polishing and magnetron sputtering technology, which can effectively reduce the cost and complexity of fabrication. To determine the sensing characteristics, a numerical computational model of the sensor based on the finite element method (FEM) is constructed using COMSOL Multiphysics software [27]. The simulation results reveal that the energy of the SPP mode is confined in the dielectric materials between the bimetallic films. Compared to the single-fiber structure, the dual D-shape WCSPR sensor shows an average sensitivity of 13,333 nm/RIU and maximum sensitivity of 52,200 nm/RIU in the refractive index range of 1.36–1.42, respectively. By further optimizing the structural parameters, an average sensitivity of 6967 nm/RIU and a figure of merit (FOM) of 222.2 RIU^{-1} were achieved in the refractive index range of 1.32–1.38, both of which were improved by more than 50 %. Notably, the loss profile at 1.34 refractive index has a FWHM as low as 9.47 nm, thus obtaining a high FOM of 327.5 RIU^{-1}, an improvement of 170 %. Among the many refractive index sensors, the dual D-shaped WCSPR sensor demonstrates a simple structure and excellent performance that promises to show great potential in the chemical and biomedical fields.

2. Principles and model

The manufacturing process of the dual D-shape WCSPR sensor is illustrated in Fig. 1. The first step is to polish off the cladding of the

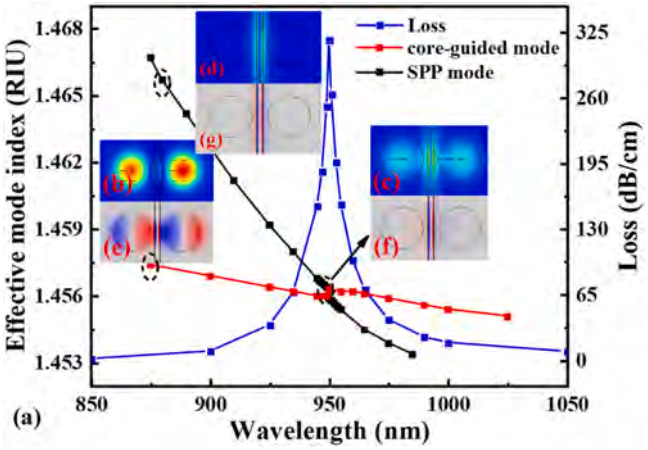

Fig. 2. (a) Dispersion relationship of the y-polarized core mode (red) and SPP mode (black) and corresponding attenuation spectrum of the y-polarized core mode (blue); (b-d) Electric field distributions of the y-polarized core mode and SPP mode in the XY plane; (e-g) Electric field distributions of the y-polarized core mode and SPP mode in the Z direction.

single-mode fiber in layers so that the light in the core can penetrate the cladding. Silver and titanium dioxide are then plated sequentially on the polished surface of the D-shape optical fiber by electroplating or magnetron sputtering [5]. The dual D-shape WCSPR sensor consists of two identical D-shape fibers, and the spacing of the coating area can be precisely regulated by the depth of the trapezoidal polishing surface. A broadband or supercontinuous light source can be used to transmit light into a single-mode fiber (SMF). The sensor can be placed directly in the analyte and the output spectrum is detected by an optical spectrum analyzer (OSA).

COMSOL Multiphysics software, based on the finite element method, is used to study the resonance conditions. Numerical simulation of the sensor characteristics requires a perfect matching layer (PML) at the boundary of the double D-type structure [28]. Incident light entering the PML layer during simulation can be absorbed and prevented from scattering, thus allowing simulation of the loss of fields in infinite space. $H = 5$ μm, $t_{Ag} = 40$ nm, and $t_{TiO2} = 25$ nm representing the distance between the polished surface and center of the core, silver film thickness, titanium dioxide thickness, respectively. The distance between the polished surfaces of the two D-types optical fibers is $t_{gap} = 1.1$ μm. Fused silica is used as the bulk materials for the optical fiber cladding and the relationship between the refractive index and wavelength is described by Sellmeier equation [29] :

$$n_{silica}(\lambda) = \sqrt{1 + \sum_{i=1}^{3} \frac{A_i \lambda^2}{\lambda^2 - B_i}} \tag{1}$$

where λ is the wavelength in micrometer, A1 = 0.6961663, A2 = 0.407943, A3 = 0.897479, $B_1 = 0.004679$, $B_2 = 0.013512$, and $B_3 = 97.934003$. The dispersion of Ag is obtained the Drude– Lorentz model [30].

$$\varepsilon_m = 1 - \frac{\lambda^2 \lambda_c}{\lambda_p^2 \left(\lambda_c + j\lambda\right)}, \tag{2}$$

where λ_p and λ_c denote the plasma wavelength and collision wavelength, respectively. The corresponding values for silver are: $\lambda_p = 1.4541 \times 10^{-7}$ m and $\lambda_c = 1.7614 \times 10^{-5}$ m. The RI of TiO_2 can is derived by the following equation [31]:

$$n_t = \sqrt{5.913 + \frac{2.441 * 10^7}{\lambda^2 - 0.803 * 10^7}} \tag{3}$$

Generally, the imaginary part of the effective refractive index $Im(n_{eff})$ is related to the transmission loss of the mode [32]:

$$\alpha_{loss} = 8.686 \times \frac{2\pi}{\lambda} Im(n_{eff}) \times 10^4 \quad (dB/cm), \tag{4}$$

where α_{loss} stands for the confinement loss, λ is the operating wavelength with a micrometer scale, and $Im(n_{eff})$represents the imaginary part of the complex RI. The peak value which represents the maximum energy transfer from the core-guided mode to the plasmon can be used to locate the resonant wavelength.

To evaluate the properties of the sensor, the three key performance parameters, namely the sensitivity, FWHM of the resonance spectra, and FOM are studied. A higher sensitivity and smaller FWHM correspond to a higher FOM indicating better quality. By means of the central wavelength of the resonance peak for different analyte refractive indexes, the wavelength sensitivity (S_λ) can be evaluated by Eq. (5) [26]:

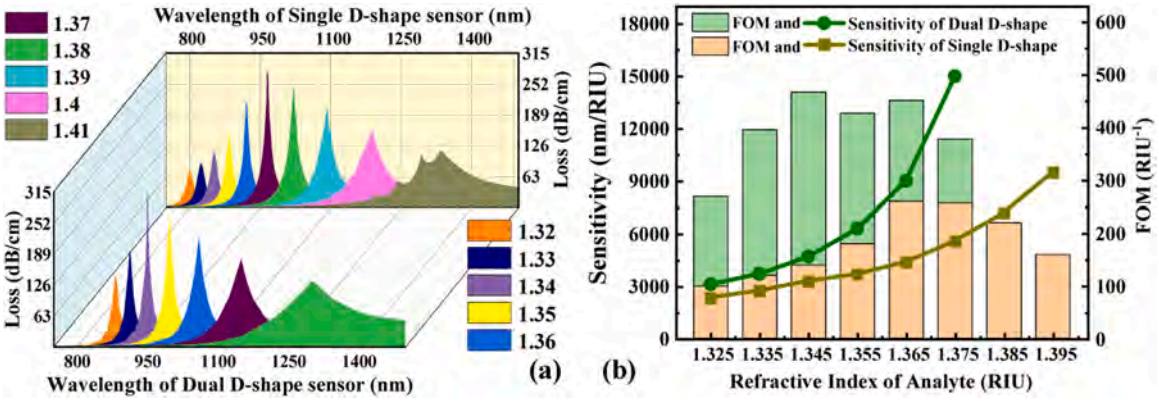

Fig. 3. (a) Loss spectrum and (b) sensitivity and FOM values of single and dual D-shape fiber optic sensors.

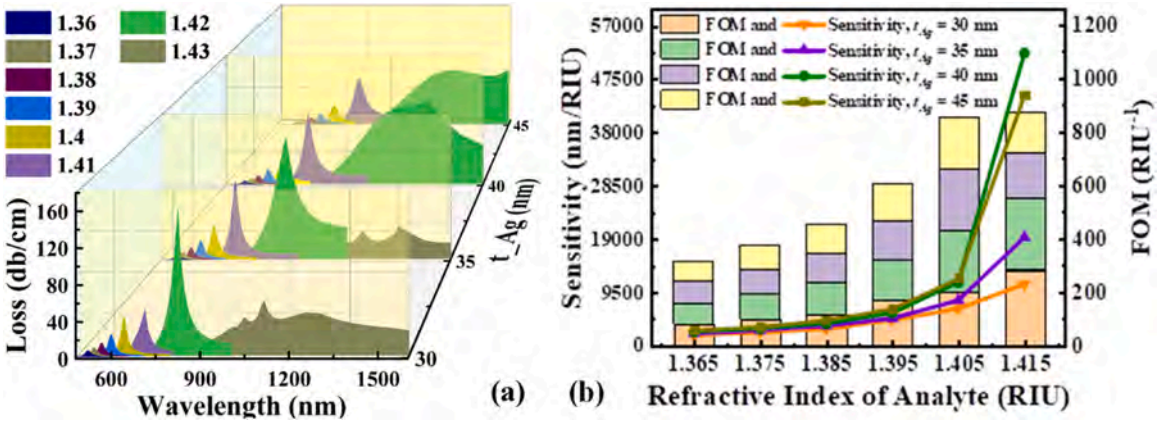

Fig. 4. (a) Loss spectra and (b) sensitivity and FOM of the dual D-shape fiber optic sensor with different silver thicknesses.

$$S_\lambda = \frac{\Delta\lambda_{peak}}{\Delta n_a}\left(\mathrm{nm}\Big/\mathrm{RIU}\right), \tag{5}$$

where Δn_a and $\Delta\lambda_{peak}$ are the variations of the analyte RI and wavelength shift of resonance peak, respectively. The properties of the SPR-based sensor are further analyzed by determining the FOM:

$$\mathrm{FOM} = \frac{S_\lambda}{\mathrm{FWHM}}\left(\mathrm{RIU}^{-1}\right) \tag{6}$$

To ensure consistency with the sensitivity in the refractive index range, the average FWHM of two adjacent resonant peaks is used to calculate the FOM.

3. Results and discussion

Fig. 2 shows SPP excitation of the sensor. By setting the refractive index of the analyte to 1.34, the fiber polishing depth and the thickness of TiO_2 and Ag to $t_{TiO2} = 25$ nm, $t_{Ag} = 40$ nm, $H = 5$ μm, respectively, and a variable gap of 1.1 μm, the eigenvalues of the guided core modes and SPP modes are simulated by sweeping the wavelength from 850 nm to 1050 nm. Owing to the asymmetrical structure of the D-shape fiber, four different core guiding modes are present. In our analysis, only the x-even mode that can be coupled with the SPP mode is investigated. As shown in Fig. 2(a), the effective refractive index dispersion relationship between core guide mode and SPP mode is shown by the blue curve. The effective refractive index of the SPP mode decreases sharply with increasing wavelength. At a wavelength of 950 nm, the core mode intersects with the SPP mode to produce an apparent loss peak indicating the strongest coupling between the core guidance mode and SPP mode. Fig. 2(b-g) depict the electric field distribution of the core-guided mode and plasmonic mode. Notably, the energy of the core guided mode transfers to the SPP mode resulting in a substantial confinement loss, as illustrated by the electric field distribution diagram of the core-guided mode at 950 nm. It is evident that light is constrained in the core guided mode and the loss is minimal at the wavelength of 875 nm. Analysis of the electric field component in the Z direction reveals that the SPP mode in the analyte results from symmetrical coupling of the SPP mode excited on both sides of the

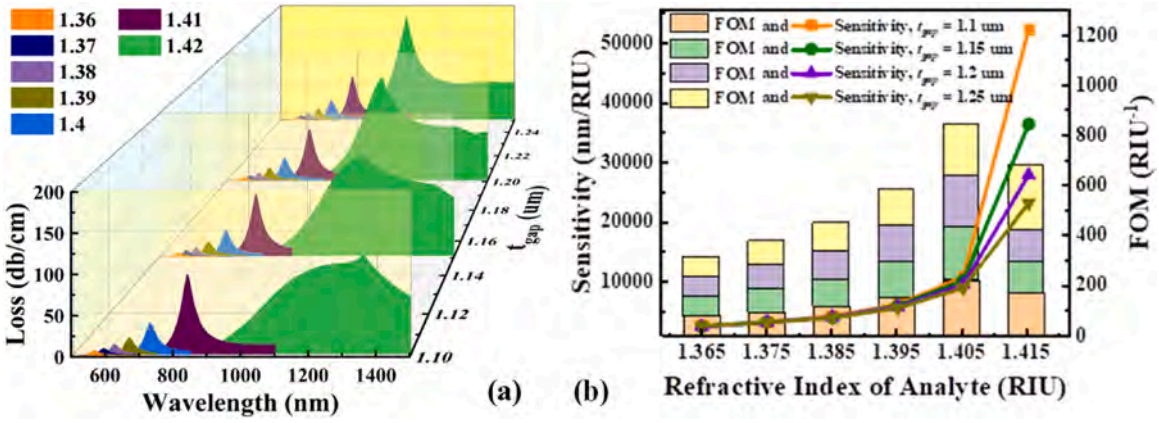

Fig. 5. (a) Loss spectra and (b) sensitivity and FOM of the dual D-shape fiber optic sensor with different variable gap.

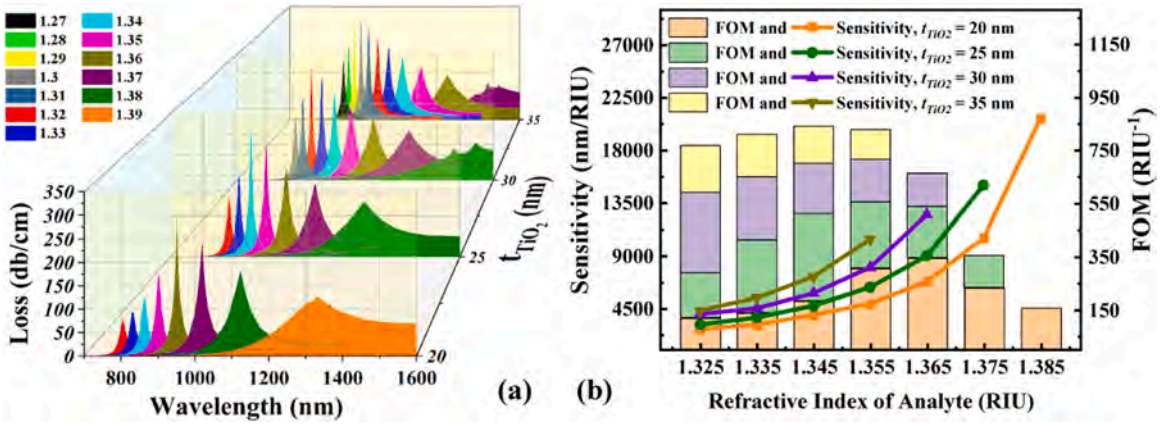

Fig. 6. (a) Loss spectra and (b) sensitivity and FOM of the dual D-shape fiber optic sensor with different TiO_2 thicknesses.

metal films in the propagation direction[33]. The dual D-shape fiber structure is able to directionally excite the SPP mode of anti-symmetric distribution of charge in the waveguide layer, unlike conventional WCSPR sensors based on metal-dielectric-metal composite structures[34]. As a result, the loss curve rapidly detaches after a sharp rise at the resonance wavelength as the wavelength increases, obtaining a narrow FWHM as low as 9.47 nm.

The loss curves and performance comparison of the designed single D-shape and dual D- shape sensors with 25 nm thick TiO_2 films are shown in Fig. 3. The WCSPR sensor is capable of achieving an average sensitivity of 6983 nm/RIU and a maximum sensitivity of 15,000 nm/RIU in the refractive index range of 1.32–1.38 with the same structural parameters. Compared with the single D-shape fiber, the average sensitivity is improved by 89.6 % and the maximum sensitivity is improved by 57.9 %. It is evident in Fig. 3(b) that the sensitivity of the WCSPR sensor is significantly due to the conventional single D-shape fiber, and the FOM value is significantly superior in the refractive index range of 1.33–1.34. Notably, the loss profile at 1.34 refractive index has a FWHM as low as 9.47 nm, thus obtaining a high FOM of 327.5 RIU^{-1}, an improvement of 170 %.

In Fig. 4, the loss spectra of the TiO_2-free dual D-shape sensor at different refractive indices are shown to investigate the effect of silver film thickness on the sensing performance. With the increase of silver film thickness, the resonance peak broadens rapidly. Also, the resonance wavelengths at 1.41 and 1.42 refractive indices are red-shifted from 706 nm and 817–838 nm and 1360 nm. Wavelength sensitivity has also been increased from 11,100 nm/RIU to a maximum of 52,200 nm/RIU. Fig. 4(b) shows that the increase in silver film thickness has a smaller effect on the FOM value and a larger effect on the sensitivity. The average sensitivity in the refractive index range of 1.36–1.42 increased from 5016.67 nm/RIU to 13,333 nm/RIU.

Fig. 5 shows the loss spectra of the dual D-shape fiber sensor without TiO_2 film with different refractive indices to investigate the effect of the spacing of the two D-shape fibers on the sensing performance. The loss curves for different refractive indices are gradually red-shifted as the fiber spacing decreases. Apparently, the loss curve changes more significantly at 1.42 refractive index, with the resonance wavelength red-shifted from 1095 nm to 1360 nm. The resonance wavelength peaks at different refractive indices are enhanced at $t_{gap} = 1.1$ μm, which is due to the smaller spacing between the metal surfaces on both sides and the higher coupling strength of the SPP mode. As shown in Fig. 5(b), despite the increase in coupling strength gained, a small range of fiber spacing variation has little effect on the wavelength sensitivity in the 1.36–1.41 refractive index range.

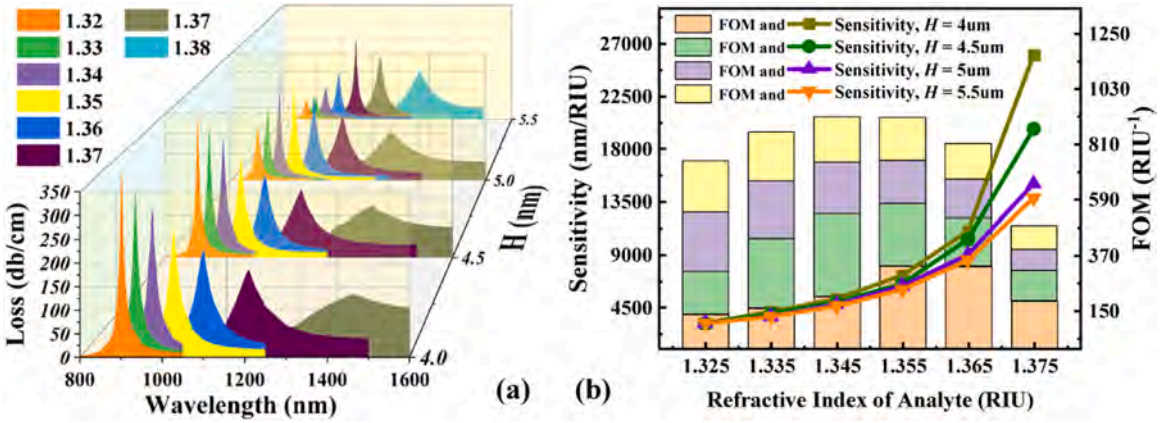

Fig. 7. (a) Loss spectra and (b) sensitivity and FOM of the dual D-shape fiber optic sensor with different *H*.

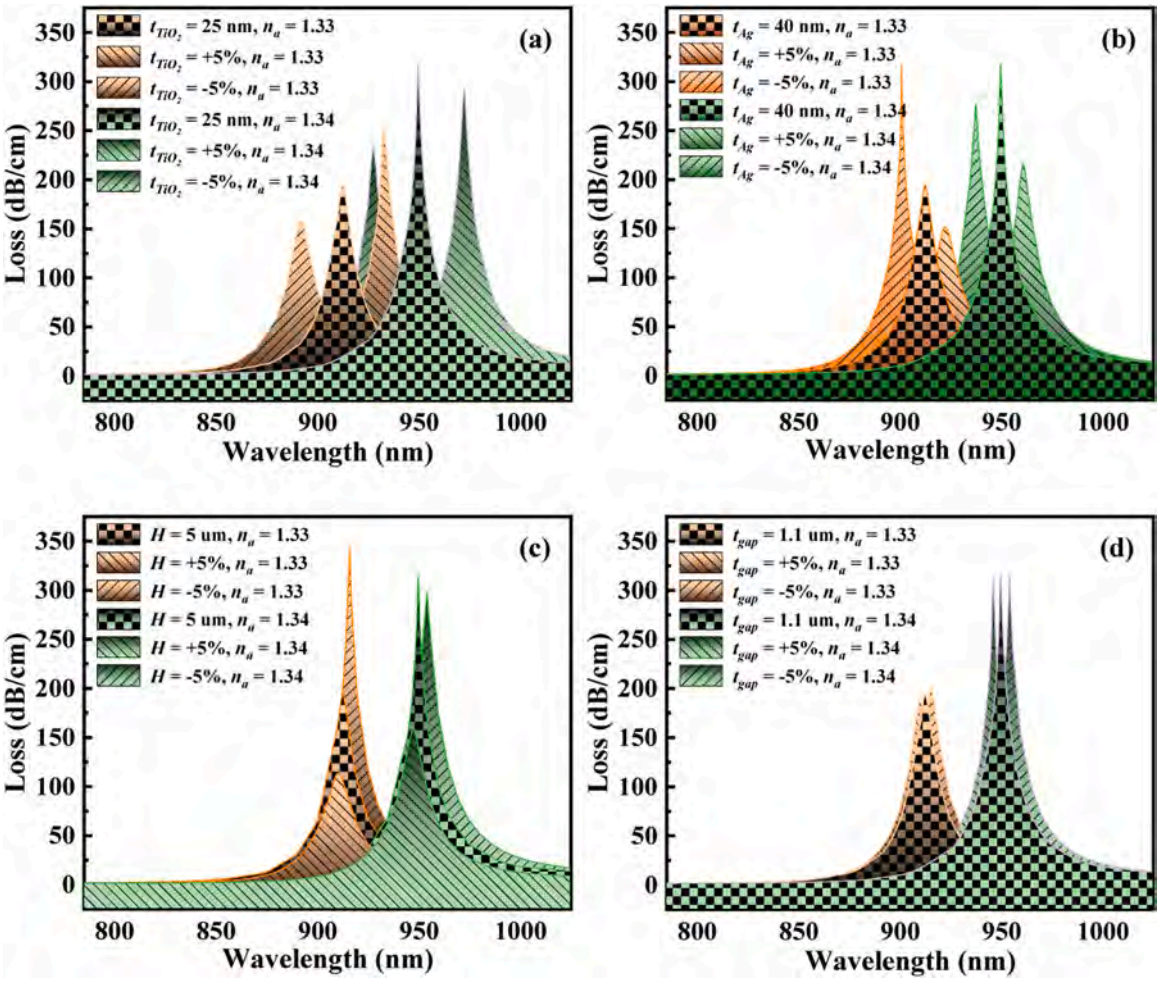

Fig. 8. Fabrication tolerance study of the proposed sensor within a tolerance of ± 5 % for TiO_2 thickness t_{TiO2} = 25 nm, silver thickness t_{Ag} = 40 nm, cladding polishing depth H = 5 μm and variable gap t_{gap} = 1.1 μm.

The effect of TiO2 film on the performance of the double-D fiber optic sensor was evaluated, as shown in Fig. 6. The loss curves, sensitivity, and FOM are determined for different TiO_2 thicknesses and refractcive indexes. As the TiO_2 film thickness goes up, the loss curves shift gradually to longer wavelengths for different refractive indexes. However, only the loss curves with resonance wavelengths

Table 1
The tolerance study of different geometric parameters within ± 5 %.

Parameter	Sensitivity (nm/RIU) & FOM (RIU^{-1})	
	+5 %	–5 %
TiO_2 thickness t_{TiO2}	3940/306.85	3600/221.8
silver thickness t_{Ag}	3850/204.08	3650/359.96
cladding polishing depth H	3650/207.86	3840/301.29
variable gap t_{gap}	3650/276.3	3900/297.26

Table 2
Comparison of the sensing properties with other reported sensors.

Sensor	RI Range	Average Sensitivity (nm/RIU)	FOM (RIU^{-1})	Ref.
Fiber/Al/Cu/DBL/analyte	1.33–1.35	6300	34	[36]
Fiber/DBL/Ag/analyte	1.33–1.41	1540	63.91	[37]
Fiber/DBL/Ag/analyte	1.333–1.363	3201	118	[13]
Fiber/Ag/DBL/analyte	1.518–1.576	6600	78	[14]
Fiber/DBL/Au/AuNPs/analyte	1.3503–1.3802	3050.19	31.12	[38]
Fiber/ DBL/Au/DBL/analyte	1.3319–1.3818	3500.6	46.55	[39]
PCF/Ag/analyte/Ag/ PCF	1.36–1.41	14,660	187	[40]
Fiber/Ag/analyte/Ag/Fiber	1.36–1.42	13,333	197	This
Fiber/Ag/TiO_2/analyte/TiO_2/Ag/Fiber	1.32–1.38	6967	222.2	work

less than 1500 nm can be utilized due to the interference peaks. Consequently, the maximum detectable refractive index of the sensor decreases from 1.39 to 1.36 and the highest sensitivity decreases from 20,700 nm/RIU to 10,400 nm/RIU when the TiO_2 thickness is increased from 20 nm to 35 nm. Interestingly, the loss curve with the lowest FWHM shifts from refractive indexes of 1.36–1.32. The TiO_2 film enhances the electric field on the metal surface, thus increasing the peak of the loss peak and improving the FOM in the sensing range. in particular, the TiO_2 film thickness of 25 nm leads to an average sensitivity of 6967 nm/RIU and an average FOM of 222.2 RIU^{-1} in the refractive index range of 1.32–1.38. Additionally, the loss curve shows an FWHM of 9.47 nm, sensitivity of 3500 nm/RIU, and FOM of 301.5 RIU^{-1} in the refractive index range of 1.33–1.35. In the refractive index range of 1.32–1.38, the sensitivity and FOM values are improved by more than 100 % compared to SPR sensors developed on single-mode fibers. Moreover, this sensor structure is not complex and can be made using ordinary side polishing techniques and single-mode fibers.

As shown in Fig. 7, loss profiles, sensitivity and FOM were determined for different H and refractive indices in order to evaluate the effect of polishing depth of the fiber cladding on the performance of the dual D-shape fiber sensor. With the increase of H, the loss curve gradually shifts to shorter wavelengths at different refractive indices. In which, the resonance wavelengths at 1.37 and 1.38 refractive indices are shifted from 1210 nm and 1470–1137 nm and 1275 nm, respectively. Also, the peak of the resonance wavelength is decreasing sharply, and it is obvious that the increase of the cladding thickness decreases the coupling strength of the guided mode and SPP mode. As shown in Fig. 7(b), the increase in cladding thickness reduces the sensitivity from 26,000 nm/RIU to 13,800 nm/RIU in the refractive index range of 1.37–1.38. However, in the refractive index range from 1.32 to 1.37, the change in cladding has little effect on the wavelength sensitivity and only has a large effect on the FOM value.

To demonstrate the manufacturing feasibility of the proposed design, a tolerance study was performed on the sensor parameters, as shown in Fig. 8 [35]. The structural parameters used for comparison have a wavelength sensitivity of 3700 nm/RIU in the refractive index range of 1.33–1.34 and a FOM value of 327.4 RIU^{-1}. Within a tolerance of ± 5 %, the resonant wavelength of the optimized parameters showed a slight shift, and the corresponding wavelength sensitivity and FOM values are shown in Table 1. Obviously, the preparation process of the plasma film will greatly affect the performance of the sensor. Among them, the thickness of TiO_2 has a large effect on the loss of resonant wavelength, and the average wavelength shifts of 1.33 and 1.34 refractive indices are 20 nm and 22 nm, respectively. but the FOM value of the proposed design is still higher than 200 RIU^{-1}, and the sensitivity variation is small.

As shown in Table 2, we compared the fiber SPR sensors of many representative sensing structures. Obviously, the WCSPR sensor with the dual D-shaped fiber structure stands out among many LRSPR and CPWR sensors with DBL because it provides a large dynamic detection range, competitive sensitivity, and FOM.

4. Conclusions

An optical SPR sensor based on two D-shape single-mode fibers is designed and analyzed by the finite element method. The unique structural design of placing the analyte in the waveguide layer greatly enhances the sensitivity to refractive index. By analyzing various structural parameters, it is found that the sensor performance is mainly affected by the fiber spacing, metal film thickness, and TiO_2 film thickness. Compared with conventional D-shape single-mode fiber SPR sensors, the average sensitivity is increased by 89.6 % and the maximum sensitivity is increased by 57.9 % in the refractive index range of 1.32–1.38. In particular, the FWHM of the loss curve at 1.34 refractive index is as low as 9.47 nm, resulting in a high FOM of 327.5 RIU^{-1}. The results show that the single-mode fiber based dual D-shape fiber WCSPR refractive index sensor have great potential for achieving low-cost in situ and label-free biosensing, among other directions.

Declaration of Competing Interest

The authors declare that they have no known competing financial interests or personal relationships that could have appeared to influence the work reported in this paper.

Data availability

Data will be made available on request.

Acknowledgments

This work was jointly supported by Heilongjiang Provincial Natural Science Foundation of China [JQ2023F001], Outstanding young and middle-aged research and innovation team of Northeast Petroleum University [KYCXTD201801], Local Universities Reformation and Development Personnel Training Supporting Project from Central Authorities, Postdoctoral scientific research development fund of Heilongjiang Province (LBH-Q20081), City University of Hong Kong Donation Research Grant [DON-RMG No. 9229021], City University of Hong Kong Strategic Research Grant [SRG 7005505], and City University of Hong Kong Donation Grant [9220061].

References

[1] C. Liu, J. Lü, W. Liu, F. Wang, P.K. Chu, Overview of refractive index sensors comprising photonic crystal fibers based on the surface plasmon resonance effect, Chin. Opt. Lett. 19 (2021), 102202.
[2] B. Yan, A. Wang, E. Liu, W. Tan, J. Xie, R. Ge, J. Liu, Polarization filtering in the visible wavelength range using surface plasmon resonance and a sunflower-type photonic quasi-crystal fiber, J. Phys. D: Appl. Phys. 51 (2018), 155105.
[3] X. Wang, J. Zhu, Y. Wu, Y. Xu, Y. Su, L. Zhang, Y. Qi, X. Wen, H. Yang, Hybrid surface plasmon effect and SERS characterization in a heterogeneous composite structure of Au nano-array and Ag film, Results Phys. 17 (2020), 103175.
[4] Y. Qi, P. Zhou, T. Zhang, X. Zhang, Y. Wang, C. Liu, Y. Bai, X. Wang, Theoretical study of a multichannel plasmonic waveguide notch filter with double-sided nanodisk and two slot cavities, Results Phys. 14 (2019), 102506.
[5] Z. Zheng, Y. Luo, H. Yang, Z. Yi, J. Zhang, Q. Song, W. Yang, C. Liu, X. Wu, P. Wu, Thermal tuning of terahertz metamaterial absorber properties based on VO 2, Phys. Chem. Chem. Phys. 24 (2022) 8846–8853.
[6] H. Chen, Z. Chen, H. Yang, L. Wen, Z. Yi, Z. Zhou, B. Dai, J. Zhang, X. Wu, P. Wu, Multi-mode surface plasmon resonance absorber based on dart-type single-layer graphene, RSC Adv. 12 (2022) 7821–7829.
[7] Y. Zeng, J. Lu, H. Fu, X. Wu, L. Yang, W. Liu, Z. Yi, Q. Liu, C. Hu, Y. Lv, HE 1, 1 mode excited surface plasmon resonance for high-sensitivity sensing by photonic crystal fibers, JOSA A 40 (2023) 35–44.
[8] F. Zhao, J. Lin, Z. Lei, Z. Yi, F. Qin, J. Zhang, L. Liu, X. Wu, W. Yang, P. Wu, Realization of 18.97% theoretical efficiency of 0.9 μm thick c-Si/ZnO heterojunction ultrathin-film solar cells via surface plasmon resonance enhancement, Phys. Chem. Chem. Phys. 24 (2022) 4871–4880.
[9] Z. Zheng, Y. Zheng, Y. Luo, Z. Yi, J. Zhang, Z. Liu, W. Yang, Y. Yu, X. Wu, P. Wu, A switchable terahertz device combining ultra-wideband absorption and ultra-wideband complete reflection, Phys. Chem. Chem. Phys. 24 (2022) 2527–2533.
[10] J. Jing, K. Liu, J. Jiang, T. Xu, S. Wang, J. Ma, Z. Zhang, W. Zhang, T. Liu, Performance improvement approaches for optical fiber SPR sensors and their sensing applications, Photonics Res. 10 (2022) 126–147.
[11] B.D. Gupta, R. Kant, Recent advances in surface plasmon resonance based fiber optic chemical and biosensors utilizing bulk and nanostructures, Opt. Laser Technol. 101 (2018) 144–161.
[12] Q. Wang, W.M. Zhao, Optical methods of antibiotic residues detections: a comprehensive review, Sens. Actuators B-Chem. 269 (2018) 238–256.
[13] H. Zhang, Y. Chen, X. Feng, X. Xiong, S. Hu, Z. Jiang, J. Dong, W. Zhu, W. Qiu, H. Guan, Long-range surface plasmon resonance sensor based on side-polished fiber for biosensing applications, IEEE J. Sel. Top. Quantum Electron. 25 (2018) 1–9.
[14] Y.-X. Jiang, B.-H. Liu, X.-S. Zhu, X.-L. Tang, Y.-W. Shi, Long-range surface plasmon resonance sensor based on dielectric/silver coated hollow fiber with enhanced figure of merit, Opt. Lett. 40 (2015) 744–747.
[15] Q. Wang, J.Y. Jing, X.Z. Wang, L.Y. Niu, W.M. Zhao, A. D-Shaped, Fiber long-range surface plasmon resonance sensor with high Q-factor and temperature self-compensation, IEEE T Instrum. Meas. 69 (2020) 2218–2224.
[16] J. Ma, K. Liu, J. Jiang, T. Xu, S. Wang, P. Chang, Z. Zhang, J. Zhang, T. Liu, All optic-fiber coupled plasmon waveguide resonance sensor using ZrS 2 based dielectric layer, Opt. Express 28 (2020) 11280–11289.
[17] J. Ma, K. Liu, J. Jiang, T. Xu, S. Wang, P. Chang, Z. Zhang, J. Zhang, T. Liu, Theoretical and experimental investigation of an all-fiber waveguide coupled surface plasmon resonance sensor with Au–ZnO–Au sandwich structure, IEEE Access 7 (2019) 169961–169968.
[18] B.-R. Huang, C.-C. Liao, C.-Y. Lu, W.-C. Ke, Y.-L. Huang, N.-C. Chen, Reduction of angular dip width of surface plasmon resonance sensor by coupling surface plasma waves on sensing surface and inside metal–dielectric–metal structure, J. Vac. Sci. Technol. A: Vac. Surf. Films 31 (2013) 06F104.
[19] J. Jing, K. Liu, J. Jiang, T. Xu, S. Wang, J. Ma, Z. Zhang, W. Zhang, T. Liu, Theoretical Investigation of Optical Fiber Waveguide Coupled Surface Plasmon Resonance Sensor with Narrow Full Width at Half-Maximum, in: 2021 19th International Conference on Optical Communications and Networks (ICOCN), IEEE, 2021, pp. 1–2.
[20] Y. Ma, F. Liu, Q. Ren, A. Zhang, FOM enhancement of a D-shaped SPR fiber sensor based on Al2O3–graphene–platinum grating, J. Opt. (2023) 1–9.
[21] Y. Dogan, R. Katirci, İ. Erdogan, E. Yartasi, Artificial neural network based optimization for Ag grated D-shaped optical fiber surface plasmon resonance refractive index sensor, Opt. Commun. 534 (2023), 129332.
[22] A. Pathak, B. Rahman, C. Viphavakit, Nanowire embedded micro-drilled dual-channel approach to develop highly sensitive biosensor, IEEE Photonics Technol. Lett. 34 (2022) 707–710.
[23] J.B. Maurya, J. Saini, A.K. Sharma, Y.K. Prajapati, A localized SPR D-shaped fiber optic sensor utilizing silver grating coated with graphene: field analysis, Opt. Fiber Technol. 75 (2023), 103204.
[24] J.Y. Jing, Q. Wang, W.M. Zhao, B.T. Wang, Long-range surface plasmon resonance and its sensing applications: a review, Opt. Laser Eng. 112 (2019) 103–118.
[25] X. Chen, W.Y. Bu, Z.F. Wu, H.J. Zhang, P.P. Shum, X.G. Shao, J.X. Pu, Near-infrared long-range surface plasmon resonance in a D-shaped honeycomb microstructured optical fiber coated with Au film, Optics Express 29 (2021) 16455–16468.
[26] W. Liu, C. Liu, J. Wang, J. Lv, Y. Lv, L. Yang, N. An, Z. Yi, Q. Liu, C. Hu, Surface plasmon resonance sensor composed of microstructured optical fibers for monitoring of external and internal environments in biological and environmental sensing, Results in Physics 47 (2023) 106365.
[27] D. Santos, A. Guerreiro, J.M. Baptista, Numerical investigation of a refractive index SPR D-type optical fiber sensor using COMSOL multiphysics, Photon. Sens. 3 (2013) 61–66.

[28] W. Liu, C. Hu, L. Zhou, Z. Yi, C. Liu, J. Lv, L. Yang, P.K. Chu, A square-lattice D-shaped photonic crystal fiber sensor based on SPR to detect analytes with large refractive indexes, Phys. E: Low. -Dimens. Syst. Nanostruct. 138 (2022), 115106.
[29] I.H. Malitson, Interspecimen comparison of the refractive index of fused silica, Josa 55 (1965) 1205–1209.
[30] A.K. Sharma, B. Gupta, On the performance of different bimetallic combinations in surface plasmon resonance based fiber optic sensors, J. Appl. Phys. 101 (2007), 093111.
[31] J.R. DeVore, Refractive indices of rutile and sphalerite, JOSA 41 (1951) 416–419.
[32] W. Liu, Y. Shi, Z. Yi, C. Liu, F.M. Wang, X.L. Li, J.W. Lv, L. Yang, P.K. Chu, Surface plasmon resonance chemical sensor composed of a microstructured optical fiber for the detection of an ultra-wide refractive index range and gas-liquid pollutants, Opt. Express 29 (2021) 40734–40747.
[33] S. Refki, S. Hayashi, A. Rahmouni, D.V. Nesterenko, Z. Sekkat, Anticrossing behavior of surface plasmon polariton dispersions in metal-insulator-metal structures, Plasmonics 11 (2016) 433–440.
[34] B. Dastmalchi, P. Tassin, T. Koschny, C.M. Soukoulis, A new perspective on plasmonics: confinement and propagation length of surface plasmons for different materials and geometries, Adv. Opt. Mater. 4 (2016) 177–184.
[35] A.M. Saber, M.F.O. Hameed, J. El-Azab, R.Y. Amer, T. Ismail, S. Obayya, Plasmonic photonic crystal fiber sensor for optical partial discharge detection, Opt. Quantum Electron. 54 (2022) 433.
[36] R. Tabassum, B.D. Gupta, Influence of oxide overlayer on the performance of a fiber optic SPR sensor with Al/Cu layers, IEEE J. Sel. Top. Quantum Electron. 23 (2016) 81–88.
[37] S. Kumar, V. Gupta, G. Sharma, G.C. Yadav, V. Singh, Investigation of silicon carbide based optical fiber coupled surface plasmon resonance sensor, Silicon 8 (2016) 533–539.
[38] Q. Wang, X.-W. Cong, Z. Cheng, W.-M. Zhao, L. Wang, X.-Y. Yin, J.-X. Jiang, Z.-H. Ren, X. Yan, A.-S. Zhu, Low dimensional nanostructure-assisted long-range surface plasmon resonance sensors with high figure of merit, IEEE Trans. NanoBioscience 22 (2022) 45–51.
[39] J.-Y. Jing, S.-Y. Li, X.-Z. Wang, Q. Zhu, F.-L. Meng, Q. Wang, A. D-type, fiber based symmetrical long-range surface plasmon resonance sensor with high quality factor, Measurement 140 (2019) 395–406.
[40] C. Liu, W. Su, Q. Liu, X. Lu, F. Wang, T. Sun, P.K. Chu, Symmetrical dual D-shape photonic crystal fibers for surface plasmon resonance sensing, Opt. Express 26 (2018) 9039–9049.